Paper No.
11192

NACE INTERNATIONAL CORROSION 2018 Conference & Expo

Investigation of $FeCO_3$ and FeS Precipitation Kinetics by EQCM

Zheng Ma, Yang Yang[(1)], Bruce Brown, Srdjan Nesic, and Marc Singer
Institute for Corrosion and Multiphase Technology, Ohio University
342 West State Street
Athens, OH, 45701
USA

ABSTRACT

Corrosion product layers play a key role in the corrosion processes by precipitating on the steel surface and can lead either to enhanced corrosion protection or, in some cases, to severe pitting, depending on the conditions. The kinetics of precipitation of corrosion product layers has a direct impact on the layers properties and their level of protectiveness. In the present study, the precipitation kinetics of iron carbonate ($FeCO_3$) and iron sulfide (FeS) were studied over a range of temperatures to gain a better understanding of their effect on corrosion resistance. An Electrochemical Quartz Crystal Microbalance (EQCM) was used to investigate the $FeCO_3$ precipitation kinetics in an aqueous CO_2 environment, as well as the FeS precipitation kinetics in an aqueous H_2S environment. In addition, different substrates were used to isolate specific aspects of the precipitation mechanisms: a cathodically polarized gold-coated quartz crystal, a cathodically polarized iron-coated quartz crystal, and a freely corroding iron-coated quartz crystal were used for $FeCO_3$ precipitation; the two latter ones were used for FeS precipitation. The measured precipitation rates in both environments were repeatable and consistent across different substrates and over the range of temperatures tested. The $FeCO_3$ precipitation rates exhibited a relatively strong dependency on system temperature and bulk saturation level of $FeCO_3$. However, FeS precipitation kinetics appeared only weakly sensitive to the change of temperature. In addition, it is also postulated that the FeS saturation level at the substrate surface (rather than in the bulk), should be taken into consideration when the bulk saturation level of FeS is relatively low. The theoretical kinetic constant and the activation energy for both $FeCO_3$ and FeS (based on bulk) were derived from the obtained EQCM results and compared with literature values.

Keywords: EQCM, iron carbonate, iron sulfide, precipitation kinetics

INTRODUCTION

Corrosion of carbon steel pipelines in oil and gas applications is often divided into two main categories: sweet corrosion that is mainly caused by aqueous carbon dioxide (CO_2), and sour corrosion which is due

---

[(1)] Current affiliation: Corrosion Management & Fabric Maintenance, BP - Gulf of Mexico Operations, Houston TX

to aqueous hydrogen sulfide (H_2S). Iron carbonate ($FeCO_3$) is the most common corrosion product that can be observed in sweet corrosions. In sour conditions, different types of iron sulfides may form depending upon the system conditions[1, 2]. In both environments, the formation of corrosion product layers plays a key role in governing the corrosion processes by serving as diffusion barrier, and by blocking the underlying metal from dissolving (when the layer is well attached to the steel surface). However, these corrosion product layers are not always protective, especially when the metal underneath is suffering from rapid corrosion. It has been suggested that the protectiveness of a corrosion product layer is dependent on the competition between the precipitation rate and corrosion rate of the underlying substrate metal[3]. Therefore, a better understanding of the factors governing the rate of corrosion product layer formation would help develop more efficient corrosion mitigation methods.

In an aqueous CO_2 environment, $FeCO_3$ precipitates from solution if the concentration product of $[Fe^{2+}]$ and $[CO_3^{2-}]$ exceeds the solubility product, $\mathrm{K_{sp,FeCO_3}}$, which is a function of temperature and ionic strength[4] as defined by Equation (1)[5]. $[\mathrm{Fe^{2+}}]_{\mathrm{eq}}$ and $[\mathrm{CO_3^{2-}}]_{\mathrm{eq}}$ are the equilibrium aqueous concentrations of $\mathrm{Fe^{2+}}$ and $\mathrm{CO_3^{2-}}$.

$$K_{sp,FeCO_3} = [Fe^{2+}]_{eq}[CO_3^{2-}]_{eq} \qquad mol^2 \cdot L^{-2} \tag{1}$$

Sun and Nesic proposed a kinetic model (S&N Model, 2008)[6] to calculate the $FeCO_3$ precipitation rate ($\mathrm{PR_{FeCO_3}}$). $\mathrm{PR_{FeCO_3}}$ is a function of the solubility limit, the saturation value of $FeCO_3$ ($\mathrm{S_{FeCO_3}}$), and temperature, as shown by Equation (2):

$$PR_{FeCO_3} = k_{r,FeCO_3} e^{-\frac{\Delta G_{FeCO_3}}{RT}} K_{sp,FeCO_3}\left(S_{FeCO_3} - 1\right) \qquad mol \cdot m^{-2} s^{-1} \tag{2}$$

where the kinetic constant $\mathrm{k_{r,FeCO_3}}$=1.8×10^6 *m^4·mol^{-1}·s^{-1}*, the activation energy of $FeCO_3$ precipitation $\Delta \mathrm{G_{FeCO_3}}$=64,851.4 *J·mol^{-1}*, and the saturation level of $FeCO_3$, $\mathrm{S_{FeCO_3}}$, is defined by

$$S_{FeCO_3} = \frac{[Fe^{2+}][CO_3^{2-}]}{K_{sp,FeCO_3}} \tag{3}$$

It has been argued[6] that the S&N model gives more realistic predictions when compared with earlier models for $FeCO_3$ precipitation rate calculations[3, 7, 8]. It is the only model that was based on the direct measurements of the precipitated $FeCO_3$ mass on steel surface, whereas the other models were relying on the indirect measurement of Fe^{2+} concentration change in the bulk solution. Furthermore, the expression for the precipitation driving force in this model is more theoretically sound: $\left(\mathrm{S_{FeCO_3}} - 1\right)$ rather than the empirical expressions that have been used by the other main models: [3, 7, 8] $\left(\left(S_{FeCO_3}\right)^{0.5} - 1\right)^2$ and $\left(S_{FeCO_3} - 1\right)\left(1 - S_{FeCO_3}{}^{-1}\right)$.

However, the S&N model was based on a crude time-averaged mass change of precipitated $FeCO_3$ which was taken before and after each exposure. To improve the accuracy of the S&N model, a more accurate technique is clearly needed, one that can monitor the *in-situ* mass change throughout the experiment duration. Besides, the S&N model was only validated at 80°C. This model needs to be validated at different temperatures to extend its validity.

Little research on FeS formation kinetics has been reported. According to Rickard, the kinetics of the formation reaction for mackinawite, one type of polymorphous of FeS that usually forms first, is of the order of milliseconds.[9, 10] At 25°C. Harmandas *et al*. [11] measured the order of precipitation rate dependence on the saturation value of FeS at 25°C and 80°C. An estimated activation energy of 40 kJ was suggested. Based on the observation from Harmandas *et al*., Lee[12] proposed an expression for mackinawite precipitation rates ($\mathrm{PR_{FeS}}$, in the unit of *mol·m*$^{-2}$*·s*$^{-1}$) calculation that includes both the effect from temperature and solution saturation of mackinawite (S_{FeS}):

$$PR_{FeS} = 11.5 \times e^{-\frac{9520.648}{T}}(S_{FeS}^{0.5} - 1)^2 \quad (4)$$

where the supersaturation for mackinawite can be calculated by:

$$S_{FeS} = \frac{[Fe^{2+}][S^{2-}]}{K_{sp,FeS(S^{2-})}} \quad (5)$$

with the $K_{sp,FeS(S^{2-})}$ being the solubility of mackinawite:

$$K_{sp,FeS(S^{2-})}=[Fe^{2+}]_{eq}[S^{2-}]_{eq} \quad (6)$$

However, Harmandas *et al*. collected the data from a homogeneous precipitation process, *i.e*. bulk precipitation. The kinetics of bulk precipitation is very different from the kinetics of a heterogeneous precipitation process on a surface, a process that occurs much more readily than homogeneous precipitation. Later on, Zheng proposed an new expression based on an analogy with the S&N $FeCO_3$ model to calculate the mackinawite layer precipitation rate[13]:

$$PR_{FeS} = 7.02 \times 10^{14} \times e^{-\frac{40000}{RT}} K_{sp,S^{2-}}(S_{FeS} - 1) \quad (7)$$

In this expression, the solubility limit of mackinawite, $\mathrm{K_{sp,S^{2-}}}$, is determined from the literature[14], and the kinetic constant $\mathrm{k_{r,Fes}}$=7.02×10^{14} *m*^{4}*·mol*$^{-1}$*·s*$^{-1}$ was used by Zheng's[(2)], what made his corrosion model perform optimally. He did not do any precipitation experimentation, and no other experimental precipitation data has been offered to support this expression, which makes its accuracy questionable without comprehensive validation. Therefore, a comprehensive understanding of the FeS layer precipitation kinetics is necessary. As a starting point, the type of FeS considered in this study is limited to mackinawite.

In the current work, a very accurate device, Electrochemical Quartz Crystal Microbalance (EQCM), was used to monitor the *in-situ* mass change. Theoretically, a nano-scale mass change on the quartz crystal surface leads to a detectable change in its oscillation frequency. According to Sauerbrey's equation[15], there is a linear relationship between the mass change on the quartz crystal surface and its oscillation frequency change:

$$\Delta f = -C_f \cdot \Delta m \quad (8)$$

[(2)] Private communication

where the Δf is frequency change (*Hz*), C_f is the sensitivity factor for the quartz crystal ($Hz \cdot \mu g^{-1} \cdot cm^2$), and Δm is the change in mass per unit area ($\mu g \cdot cm^{-2}$).

Besides the ability of monitoring the *in-situ* mass change in high resolution, the EQCM also allows simultaneous electrochemical measurements. This makes the EQCM a good tool for the current work.

EXPERIMENTAL

Methodology

The methodology developed for using the EQCM to study the precipitation kinetics of both $FeCO_3$ and FeS is presented in this section. In order to differentiate the various effects on corrosion precipitation as detected by the EQCM mass change, different substrates were used: polarized Au-coated quartz crystal, cathodically protected Fe-coated quartz crystal, and actively corroding Fe-coated quartz crystal. These substrates all had advantages and disadvantages that are discussed below.

- The polarized Au-coated quartz crystal was used so that the precipitation was the only process that affected the EQCM measurements since Au is inert in these test conditions. To simulate the corrosion potential and surface water chemistry seen with carbon steel corroding under similar conditions, a cathodic polarization was applied on the crystal.
- The Fe-coated quartz crystal is closer in nature to the carbon steel surface, and the cathodic polarization was used to minimize the effect of substrate corrosion and to ensure the precipitation was the dominant process during the measurement.
- The precipitation kinetics of corrosion product on an actively corroding Fe-coated quartz crystal was also measured to simulate the most realistic situation as both of the precipitation and spontaneous iron corrosion were occurring on the substrate surface simultaneously. However, this made distinguishing mass loss by corrosion from mass gain by precipitation harder.

Furthermore, the experiments were performed at different temperatures so that the effects on the precipitation kinetics of $FeCO_3$ and FeS could be defined over a wider range of conditions.

In the case of $FeCO_3$ precipitation, three sets of experiments were conducted on polarized Au-coated quartz crystal surface, cathodically protected Fe-coated quartz crystal surface, and actively corroding Fe-coated quartz crystal surface. The results were compared with S&N model's predictions. High initial saturation of $FeCO_3$ was used in the related experiments to speed up this relatively slow process.

For the FeS precipitation, both cathodically protected Fe-coated quartz crystal surface and actively corroding Fe-coated quartz crystal surface were used. The Au-coated quartz crystal was not used as it could not provide repeatable results. High initial saturation of FeS was not required as the FeS precipitation kinetics is much faster than that of $FeCO_3$.

Apparatus

The EQCM device by Stanford Research System (QCM200) was used. The Au-coated and Fe-coated quartz crystals with a 1.37 cm^2 effective area are shown in Figure 1. Before the experiment, the quartz crystal was installed into the crystal holder and immersed into a 2-liter glass cell (shown in Figure 2) to serve as the working electrode. A saturated Ag/AgCl electrode was used as the reference electrode and the counter electrode was a platinum wire mesh as shown in the figure. The solution pH was monitored through a pH probe immersed in the electrolyte. A desired CO_2 or H_2S concentration was maintained by

a sparge tube through the entire duration of the experiment. A thermocouple was also immersed in solution and connected to a heating plate to control the temperature of the electrolyte.

Figure 1: Gold-coated (left) and iron-coated (right) quartz crystal

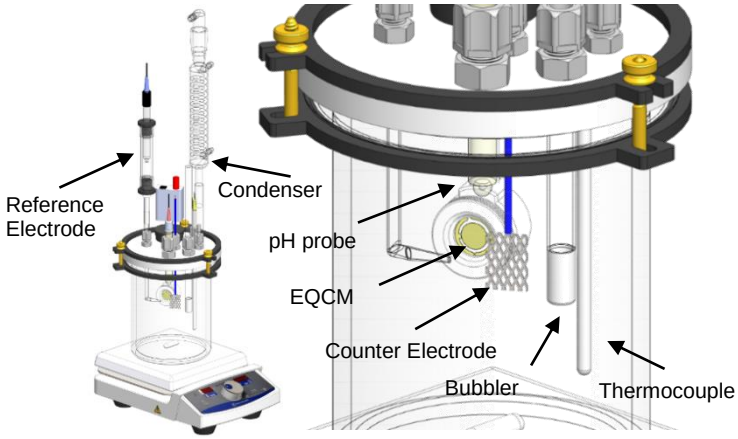

Figure 2: Experimental set-up with EQCM (Image courtesy of Cody Shafer, ICMT).

Procedure

The experimental matrix for the three sets of $FeCO_3$ precipitation experiments is shown in Table 1. All the experiments were conducted in a 2-liter glass cell filled with 1wt.% NaCl solution. CO_2 gas was sparged before and during the test to remove oxygen and maintain a saturated CO_2 environment. After the solution temperature was set to the desired value, the solution pH was adjusted to 6.6 by adding a deoxygenated $NaHCO_3$ solution. The quartz crystal was cleaned with a N_2 gas stream before each test to remove any dust from the surface. The working electrode potential was adjusted using a potentiostat (Gamry Reference 600^{TM†}). A deaerated ferrous chloride ($FeCl_2 \cdot 4H_2O$) solution was added to adjust the Fe^{2+} concentration i.e. the level of $FeCO_3$ or FeS supersaturation. Solution samples were drawn periodically from the glass cell to record the change in the bulk pH and Fe^{2+} concentration. When using the actively corroding iron coated quartz crystal, linear polarization resistance (LPR) was employed to measure the corrosion rate using a B value of 26 mV. The surface of the quartz crystal specimen was taken out for analysis by scanning electron microscope (SEM) after the experiment.

The experimental matrix covering the two sets of FeS precipitation experiments is shown in Table 2. The experimental procedure of FeS precipitation was very similar to that of $FeCO_3$ precipitation with three differences: instead of using CO_2, the solution was de-aerated by sparging with N_2 for at least two hours,

---

† Trade Name

followed by sparging with a mixture of H_2S/N_2 to saturate the bulk solution at a desired H_2S partial pressure; to adjusted the solution pH, a deoxygenated NaOH solution was added instead of a $NaHCO_3$ solution; higher stirring speed was employed during FeS precipitation to improve the mixing in the electrolyte and prevent buildup of unreasonably high local S_{FeS} at the steel surface and uncontrollable precipitation rates.

Table 1
Experimental Matrix for $FeCO_3$ Precipitation on Different Substrates.

Description	Parameters			
Solution	1wt.% NaCl			
Total pressure/ bar	1			
Purging gas	CO_2			
Initial solution pH	6.6±0.05			
Stir bar stirring speed/rpm	50			
Materials	Etched Au-coated quartz crystal	Polished Fe-coated quartz crystal	Polished Fe-coated quartz crystal	
Polarization	-0.68 V *vs.* Sat. Ag/AgCl	-0.05~-0.1 V *vs.* OCP	None (0 V *vs.* OCP)	
Temperature/°C	60, 70, 80	50, 60, 70, 80	50, 60, 70	80
Initial S_{FeCO_3}	~600	~600	~600	160, 300, 450, 600

Table 2
Experimental Matrix for FeS Formation on Different Substrates.

Description	Parameters		
Solution	1wt.% NaCl		
Total pressure/bar	1		
H_2S partial pressure/ppm	100		
Initial solution pH	6.6±0.05		
Stir bar stirring speed/rpm	250		
Materials	Polished Fe-coated quartz crystal		
Temperature/°C	30	40	50
Initial $[Fe^{2+}]$/ppm	15~30		
Polarization/V	-0.05~-0.1 vs. OCP	None (0 vs. OCP)	

Procedure for $FeCO_3$ and FeS Precipitation Rate Calculation

The precipitation rates of $FeCO_3$ and FeS from EQCM measurement were calculated by using the same methodology, illustrated in Figure 3 by using an example of $FeCO_3$ precipitating on a polarized Au-coated quartz crystal. During the experiment, the pH value and Fe^{2+} concentration in the bulk solution were measured multiple times to get the bulk saturation values of $FeCO_3$ according to Equation (3) or the bulk saturation value of FeS according to Equation (5). Given that the accuracy of measuring the Fe^{2+} concentration was up to 1% of the measurement range, and the accuracy of the pH measurement was approximately 0.1 pH unit, 12% error bars were added to all the graphs below to represent an estimated error in determining the saturation value. The error in measuring the mass change using the EQCM was not accounted for as the error was too small to be adequately shown on the plots.

As shown in Figure 3, the mass change monitored by EQCM increased due to the $FeCO_3$ precipitated on the surface of the quartz crystal. Each time when the saturation of $FeCO_3$ was measured, the instantaneous slope (mass changes per unit area *vs*. time) at those specific times was calculated and used to determine the precipitation rate and the corresponding saturation value. The measured precipitation rates having the unit of $\mu g \cdot cm^{-2} \cdot s^{-1}$ were converted to $mol \cdot m^{-2} \cdot s^{-1}$ for easier comparison with literature data[6, 13]. Even though the precipitation is a two-step process that includes both crystal nucleation and crystal growth[16] , the current work aims at finding the precipitation rate during crystal growth period only, as the nucleation step is usually short and surface preparation dependent[17]. In addition, the crystal growth step is a process that is more relevant to the understanding of the corrosion product layers formation[18] .

When using an actively corroding Fe-coated quartz crystal, the calculated precipitation rate would appear to be lower than its true value if the EQCM captured mass gain were to be used directly without compensation for mass loss due to corrosion. The total mass change captured by the EQCM is equal to the precipitation mass gain minus the corrosion mass loss. A mass compensation protocol was put in place to address this issue whenever an actively corroding Fe-coated quartz crystal was used (except the results obtained at 80°C for which corrosion rates were not measured): the mass loss was calculated from the LPR measured corrosion rate data and then added to the mass gain recorded by EQCM. The obtained new value was used for precipitation rate calculation.

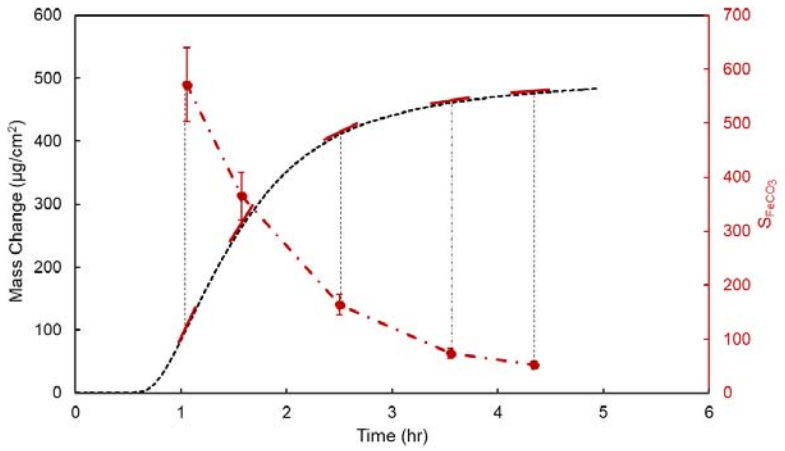

Figure 3: Illustration of $FeCO_3$ precipitation rate calculation methodology using EQCM on a polarized Au-coated quartz crystal, pH 6.6, initial S_{FeCO_3}=600, 80°C.

Validation of the Precipitation Rate Measurement Methodology

The precipitation rate measurement methodology using EQCM described above was validated by comparing with the S&N model's calculation at 80°C as shown in Figure 4. This specific temperature was chosen as it was the only temperature that S&N used to validate the model with their experimental measured precipitation rates. In the current study, an initial S_{FeCO_3} around 600 was used for both polarized Au-coated quartz crystal and polarized Fe-coated quartz crystal. When using the actively corroding Fe-coated quartz crystal, the precipitation tests were repeated starting with four different initial S_{FeCO_3}as noted in Table 1. In general, a reasonable agreement was reached between the EQCM measured precipitation rate and S&N model's calculation, given that the difference between the model prediction and measurements was of the same order of magnitude as the variation within the different measurements. Additionally, the EQCM experimental results showed reasonable consistency, *i.e.,* they were similar in magnitude, even though different substrates were used. Furthermore, a similar exponent with respect to $S_{FeCO_3}$of approximately 1 was obtained on all substrates. This supports the linear relationship between the $FeCO_3$ precipitation rate and S_{FeCO_3} as described in the S&N model. Overall, it can be concluded that the EQCM technique was validated for the precipitation rate measurements.

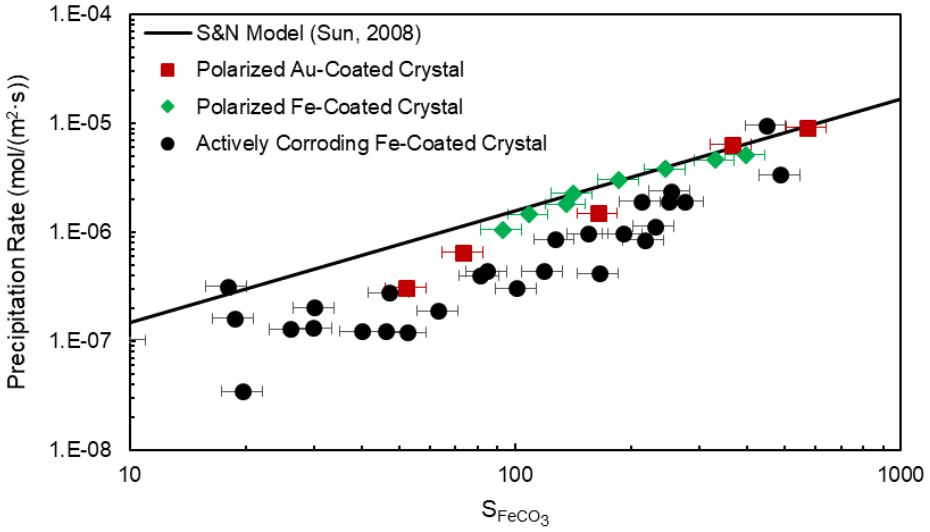

Figure 4: Comparison between S&N model calculation and EQCM experimental results on different substrates at 80°C, pH 6.6.

EXPERIMENTAL RESULTS AND DISCUSSION

Precipitation Rate of $FeCO_3$

The experimental results related to $FeCO_3$ precipitation kinetics measured by EQCM over a broad range of temperatures (50 – 80°C) are pending publication elsewhere[19]. However, the main results are briefly reviewed in this section to facilitate comparison with the precipitation kinetics of FeS.

When precipitating on a polarized Au-coated quartz crystal, the difference between the EQCM results and model's predictions was more significant at lower temperature: the best average agreement with the model was found at 80°C as shown in Figure 4. The model's calculation was about 60% higher than the EQCM results when the temperature decreased to 70°. At 60°C, the EQCM measured precipitation rate

was about an order of magnitude lower than model's calculation, and about 2-3 times lower than the results obtained from the other two substrates. It was postulated that the Au-coated quartz crystal substrate artificially affected the nucleation process; this became more prominent and retarded the kinetics of the entire precipitation process at a lower temperatures. The precipitation kinetics was affected less by the relatively slow nucleation process at higher temperature, since the overall precipitation kinetics was faster. At 50°C, it was impossible to conduct a repeatable precipitation experiment on Au-coated quartz crystal.

The precipitation rates measured on actively corroding Fe-coated quartz crystal appeared to be in much better agreement with the S&N model's calculation when compared with what was found on polarized Au-coated quartz crystal. However, most of the measured precipitation rates on this type of substrate were considerably lower than the ones obtained on polarized Fe-coated quartz crystal up to a factor of two, at all the tested temperatures. This is because the results were altered by two competing processes that occur on the actively corroding substrate surface during the measurement: extra Fe^{2+} is generated at the substrate surface due to the corrosion process, increasing the surface $FeCO_3$ saturation level and making the precipitation rate faster; concurrently, a corroding Fe surface continuously undermined the substrate surface and made it harder for $FeCO_3$ to nucleate. These difficulties rendered the actively corroding Fe-coated quartz crystal a less than ideal substrate for measuring the $FeCO_3$ precipitation kinetics as it was difficult to resolve which of these effects dominated the precipitation process.

The cathodic polarization that was applied to the Fe-coated crystal made the polarized Fe the most suitable surface to measure the precipitation kinetics since the effect of Fe dissolution was greatly reduced. Theoretically, the surface pH close to the substrate surface was also increased by applying the cathodic polarization and this increased the surface S_{FeCO_3}. However, the precipitation rate measured on this substrate surface presented the best agreement between the EQCM results and S&N model for all the tested temperature. This suggests that the variations at substrate surface had a minor effect on the $FeCO_3$ precipitation kinetics under the high bulk S_{FeCO_3} conditions tested.

When the temperature was decreased to 40°C, the repeatability of the experiments was rather poor even using the polarized Fe-coated crystal. The overall precipitation process became slow, erratic and irreproducible due to the low temperature

Precipitation Rate of FeS

FeS was precipitated on both cathodically polarized Fe-coated crystal and actively corroding Fe-coated crystal at different temperatures as shown in Table 2. The bulk Fe^{2+} concentration was stable during the entire duration of the FeS precipitation measurements but the pH decreased significantly (anywhere between 0.5 to 2 pH unit). This caused a fast decrease of S_{FeS} as the $[S^{2-}]$ in Equation (**5**) decreases with a lower solution pH. This was different from what had been seen in the $FeCO_3$ precipitation experiments where the solution pH change was minor (within 0.2 pH unit) because of the stronger buffering effect from H_2CO_3, and where the S_{FeCO_3} decreased mainly due to the decrease of Fe^{2+} concentration in the bulk solution.

Figure 5 shows the change of EQCM measured mass and S_{FeS} in the bulk solution *vs.* the time on a polarized Fe-coated crystal at 30°C. As can be seen from the figure, the S_{FeS} in the bulk solution, $S_{FeS,bulk}$, appeared to drop below 1 after 10 hours and became lower than 0.01 after 30 hours. During the entire experimental window, the EQCM mass gain was increasing even when the $S_{FeS,bulk}$ was much lower than 1. The same phenomenon was observed at all the tested temperatures. This seems physically impossible as the precipitation could not have continued when the S_{FeS} reached 1 (saturation). By the same token,

the precipitation of FeS could not have led to a decrease of S_{FeS} below 1. However, with the increased pH at the substrate surface caused by the cathodic polarization, it is likely that the S_{FeS} at the substrate surface, $S_{FeS,surface}$, was much higher than 1 and thus promoted the FeS precipitation while at the same time $S_{FeS,bulk}$ was smaller than 1.

Based on this observation, it can be concluded that, in order to study the precipitation kinetics of FeS, the S_{FeS} on the substrate surface ($S_{FeS,surface}$) should be taken into consideration, especially when the precipitation takes place in a solution with a relative low $S_{FeS,bulk}$. This is different from the $FeCO_3$ precipitation where bulk conditions, rather than those at the substrate surface, qualify the process better. This is due to the fact that the $FeCO_3$ precipitation kinetics is fairly slow as it has a relatively high activation energy[6]. A high S_{FeCO_3} in the bulk solution is necessary to trigger the process and since the S_{FeCO_3} in the bulk solution was really high, the bulk solution chemistry was not all that different from the solution chemistry at the substrate surface, both being highly supersaturated. In contrast, the FeS precipitation kinetics is much faster and a much lower $S_{FeS,bulk}$was used in H_2S experiments, when compared to the $S_{FeCO_3,bulk}$ used for $FeCO_3$ precipitation kinetics study. Under such conditions, $S_{FeS,bulk}$ was very different from the $S_{FeS,surface}$ at the surface which was much higher. This meant that the surface $S_{FeS,surface}$ needed to be considered in the FeS precipitation kinetics study, which was not readily measurable.

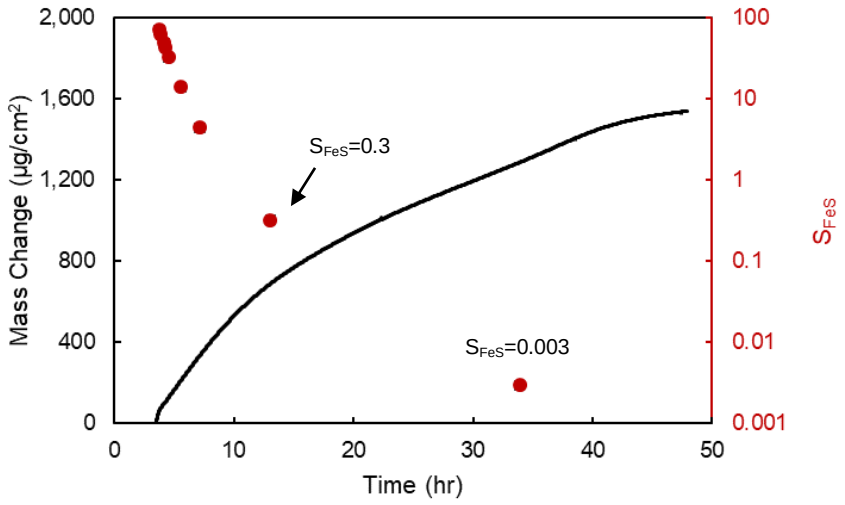

Figure 5: Mass change and S_{FeS} change vs. time on polarized Fe-coated crystal, 30°C.

The calculated precipitation kinetics of FeS on a polarized Fe-coated crystal are shown in Figure 6 for 30°C. Generally, PR_{FeS} decreased with the decrease of the $S_{FeS,bulk}$. However, as has been discussed above, further study of the effect of surface process on the PR_{FeS} is required to reach a better understanding on the relationship between S_{FeS} and PR_{FeS}.

Figure 7 presents the calculated PR_{FeS} *vs.* $S_{FeS,bulk}$ on an actively corroding Fe-coated crystal at 30°C. Both PR_{FeS} before and after the mass compensation are included. It can be seen that the PR_{FeS} was up to 10 times lager after applying compensation for the total mass change and was affected more by the compensation at lower $S_{FeS,bulk}$. This suggests that the mass loss due to corrosion was much higher than the EQCM measured mass gain, especially at lower $S_{FeS,bulk}$. The best fit line is included in the figure for the compensated result to show the relationship between the PR_{FeS} and the $S_{FeS,bulk}$. The exponent value with respect to $S_{FeS,bulk}$ of 0.19 is obtained, indicating a very weak dependency between PR_{FeS} and

$S_{FeS,bulk}$. However, one needs to keep in mind that the $S_{FeS,bulk}$ in the bulk was very different from the $S_{FeS,surface}$ at the substrate surface. The PR_{FeS} needs to be correlated with $S_{FeS,surface}$rather than the $S_{FeS,bulk}$, however the former is not readily measurable.

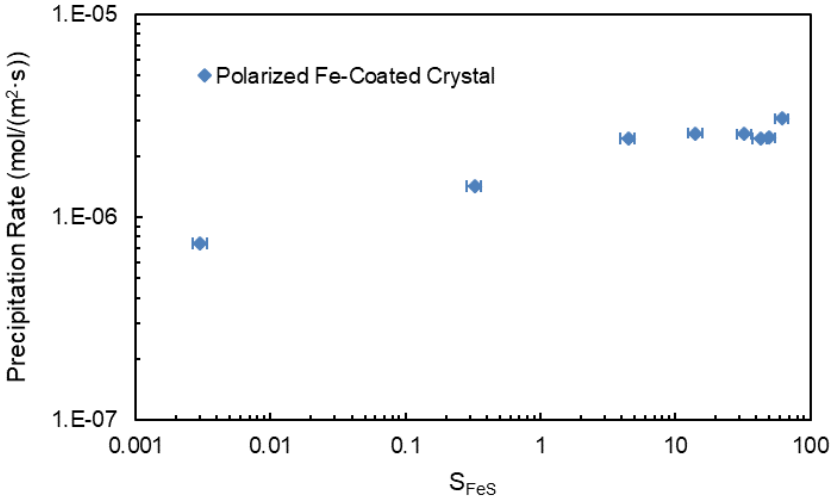

Figure 6: Precipitation kinetics of FeS on polarized Fe-coated crystal, 30°C.

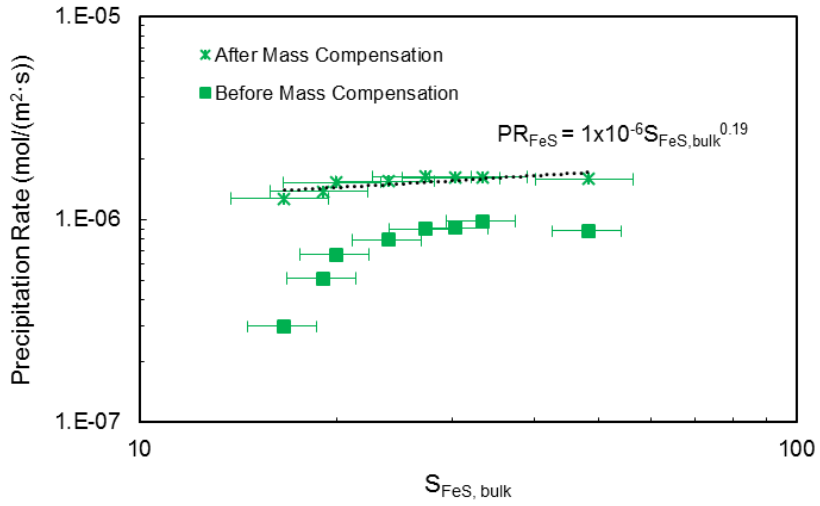

Figure 7: Precipitation kinetics of FeS on actively corroding Fe-coated crystal, before and after mass compensation, 30°C.

The PR_{FeS} obtained from the polarized Fe-coated crystal (Figure 6) and the compensated actively corroding Fe-coated crystal (Figure 7) at 30°C and for $S_{FeS,bulk}$>10 are compared in Figure 8. The PR_{FeS} on the polarized Fe-coated crystal is generally higher than those obtained from compensated actively corroding Fe-coated crystal and this difference gets larger at lower $S_{FeS,bulk}$. This phenomenon agrees with what have been observed during the precipitation of $FeCO_3$ as explained in the previous section. Given the fact that the heterogeneous precipitation is notoriously difficult to reproduce, a 60% average difference in precipitation rates measured on the two substrate surfaces is acceptable.

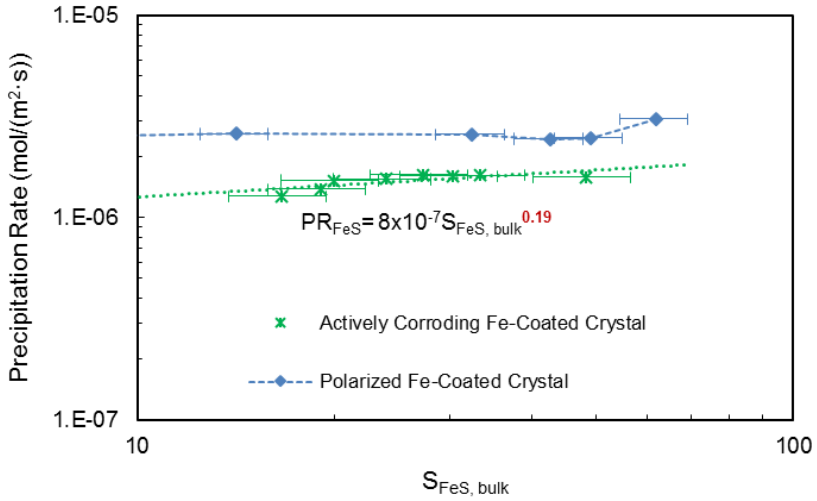

Figure 8: Precipitation kinetics comparison of FeS on both substrates, 30°C.

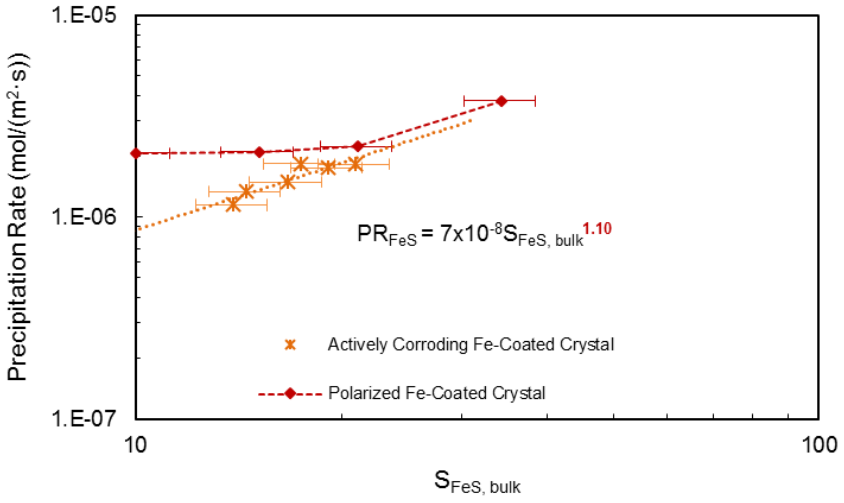

Figure 9: Precipitation kinetics comparison of FeS on both substrates, 40°C.

The PR_{FeS} obtained for both the compensated actively corroding Fe-coated crystal and the polarized Fe-coated crystal at 40°C and for $S_{FeS,bulk} > 10$ are shown in Figure 9. Similar to the results at 30°C, the PR_{FeS} on different substrates agree better with each other at higher $S_{FeS,bulk}$ and the discrepancy between the two different substrate surfaces becomes larger with the decrease of the $S_{FeS,bulk}$. The best fit line and equation are included based on the results obtained from compensated actively corroding Fe-coated crystal and the exponent value with respect to bulk S_{FeS} of approximately 1 was obtained. This indicates almost a linear relationship between PR_{FeS} and $S_{FeS,bulk}$ under this condition. The raw data for the actively corroding Fe-coated crystal without compensation was not included in the figure as it did not provide useful information. However, it is noted that the PR_{FeS} was up to 5 times larger after applying compensation for the total mass change.

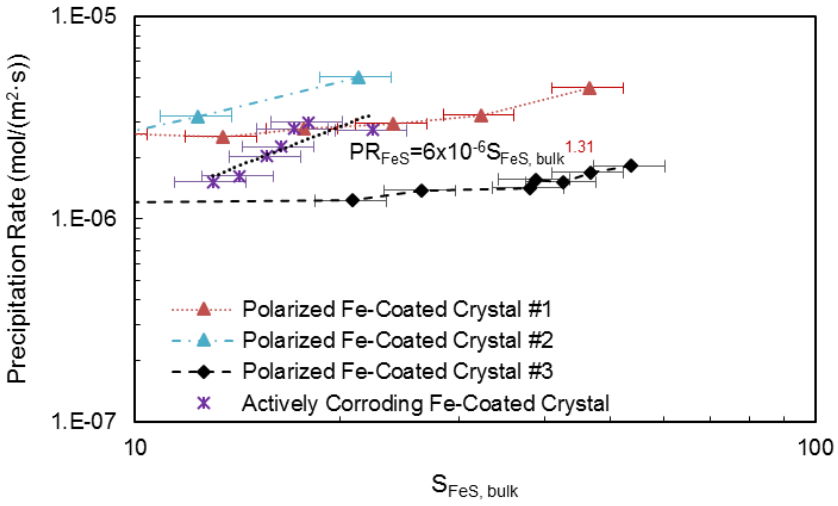

Figure 10: Precipitation kinetics comparison of FeS on both substrates, 50°C.

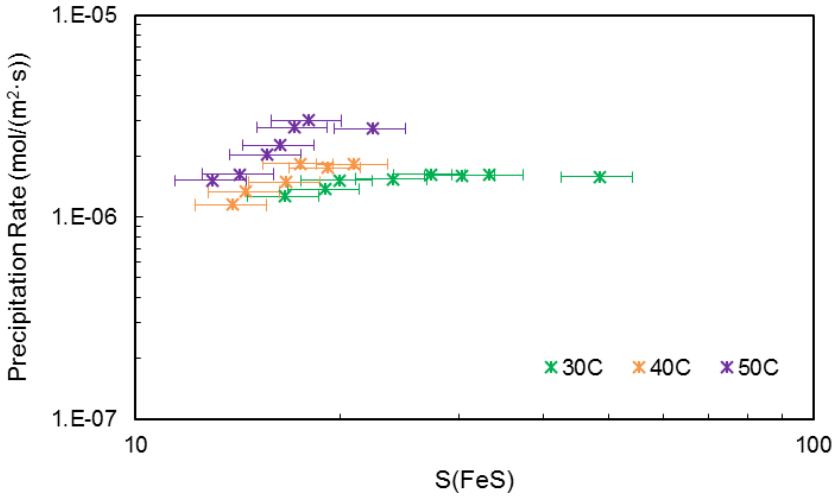

Figure 11: Compensated precipitation kinetics of FeS at different temperatures.

A similar comparison of PR_{FeS} *vs.* $S_{FeS,bulk}$ for the polarized Fe-coated crystal and for the compensated actively corroding Fe-coated crystal at 50°C and $S_{FeS,bulk} > 10$ is presented in Figure 10. The experiment was repeated three times on the polarized Fe-coated crystal using the same environmental conditions. The results exhibit reasonable consistency, with most of the results being within a factor of 4 of each other. When using the actively corroding Fe-coated crystal, the compensated PR_{FeS} was up to 4 times larger than the one without using mass compensation (not shown in the figure). The exponent value with respect to $S_{FeS,bulk}$ of approximately 1.31 was obtained based on the results from the compensated actively corroding Fe-coated crystal. In addition, the PR_{FeS} on the compensated actively corroding Fe-coated crystal are within the margin of error of the results obtained on the polarized Fe-coated crystal and they have the same order of magnitude.

Comparison of the compensated PR_{FeS} *vs.* $S_{FeS,bulk}$ at different temperatures from 30°C to 50°C is shown in Figure 11. When comparing at similar $S_{FeS,bulk}$ values, the PR_{FeS} at 50°C was barely two times higher than that at 30°C. This suggests a weak temperature dependency of FeS precipitation kinetics.

ACTIVATION ENERGY AND KINETIC CONSTANT IN THE PRECIPITATION RATE EQUATIONS

Precipitation Rate Equation of $FeCO_3$

The activation energy and kinetic constant for $FeCO_3$ can be extracted from the previously presented EQCM results by taking a natural logarithm of both side of Equation (2):

$$ln\frac{PR_{FeCO_3}}{K_{sp,FeCO_3}\cdot(S_{FeCO_3}-1)} = -\frac{\Delta G_{FeCO_3}}{RT} + ln\, k_{r,FeCO_3} \tag{9}$$

When plotting $ln\frac{PR_{FeCO_3}}{K_{sp,FeCO_3}\cdot(S_{FeCO_3}-1)}$ *vs.* $(-\frac{1}{RT})$, the activation energy ΔG_{FeCO_3} can be obtained from the slope of the straight line and the $\ln k_{r,FeCO_3}$ can be determined from the y intercept as shown in Figure 12. By using the average experimental value at each temperature, the best fit line yielded ΔG_{FeCO_3}=73739 *J·mol*$^{-1}$ and $k_{r,FeCO_3}$=3.32×10^7 *m*^{4}*·mol*$^{-1}$*·s*$^{-1}$. When comparing with the constants that have been reported in S&N's $FeCO_3$ model (64,851.4 *J·mol*$^{-1}$ and 1.8×10^6 *m*^{4}*·mol*$^{-1}$*·s*$^{-1}$), a higher activation energy and a higher kinetic constant were obtained here based on the EQCM results. When comparing the experimental $FeCO_3$ precipitation rate results with the calculated $FeCO_3$ precipitation rate results from the current model with the new constants and S&N model, an improvement was achieved particularly at the lower saturation levels[19].

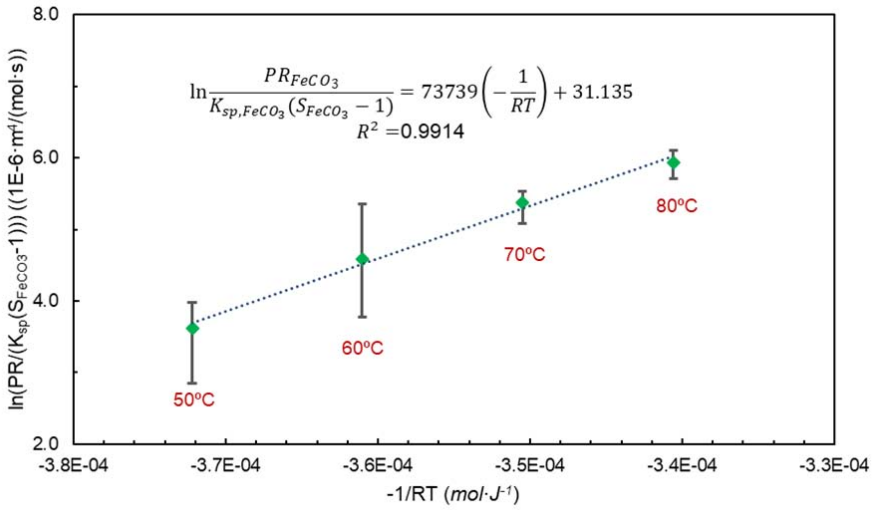

Figure 12: The best fit line for activation energy and kinetic constant in the $FeCO_3$ precipitation rate equation. Adapted from Ma *et al.*[19].

Precipitation Rate Equation of FeS

The precipitation kinetics measured on different substrates generally agreed with each other over the range of temperatures used, when the $S_{FeS,bulk}$ was higher than 10. This is because the complications

due to surface effects on PR_{FeS} were not as dominant at higher $S_{FeS,bulk}$. By analogy to the work done on $FeCO_3$ precipitation, an FeS precipitation rate model is proposed based on the compensated results from 30°C to 50°C. The theoretically correct exponent value with respect to $S_{FeS,bulk}$ of 1 is used to represent the linear relationship between PR_{FeS} and $S_{FeS,bulk}$:

$$PR_{FeS}\left(\frac{mol}{m^2 s}\right) = k_{r,FeS} e^{-\frac{\Delta G_{FeS}}{RT}} K_{sp,FeS}\left(S_{FeS,bulk} - 1\right) \quad (10)$$

where $k_{r,FeS}$ is kinetic constant ($m^4 \cdot mol^{-1} \cdot s^{-1}$), and ΔG_{FeS} is the activation energy of FeS precipitation ($J \cdot mol^{-1}$).

By adopting a similar procedure as shown in the previous section, the best fit line yielded ΔG_{FeS} = 35,284 $J \cdot mol^{-1}$ and $k_{r,FeS}$= 5.88×10^{13} $m^4 \cdot mol^{-1} \cdot s^{-1}$ by using the average experimental value at each temperature (Figure 13). The activation energy is slightly lower than that of Harmandas *et al.*'s (40,000 $J \cdot mol^{-1}$)[11]. However, one needs to keep in mind that the current research refers to the heterogeneous precipitation on a substrate while the literature data are from a homogeneous precipitation process and that precipitation rate of FeS was measured indirectly.

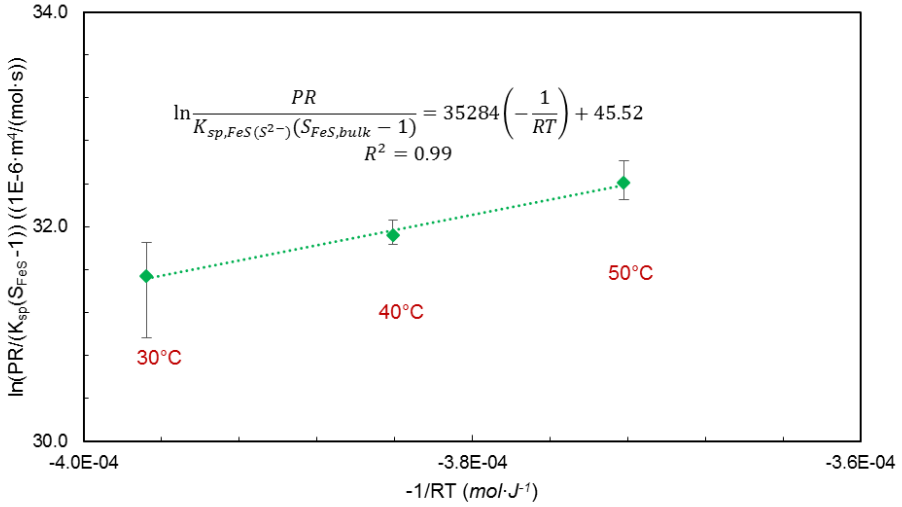

Figure 13: The best fit line for activation energy and kinetic constant in the FeS precipitation rate equation.

It can be seen that the required activation energy for FeS precipitation is about 50% of that for $FeCO_3$ precipitation (35,284 $J \cdot mol^{-1}$ *vs.* 73,739 $J \cdot mol^{-1}$). This suggests that the sensitivity of $FeCO_3$ precipitation to temperature is higher than that of FeS. Comparison of kinetic constants ($k_{r,FeS}$=5.88×10^{13} $m^4 \cdot mol^{-1} \cdot s^{-1}$ *vs*. $k_{r,FeCO_3}$=3.32×10^7 $m^4 \cdot mol^{-1} \cdot s^{-1}$) shows that FeS precipitation is much faster. The precipitation kinetics of FeS and $FeCO_3$ at the same temperature are compared in Figure 14. At the same bulk saturation value as $FeCO_3$, the precipitation rate of FeS is close to two orders of magnitude higher than that of $FeCO_3$.

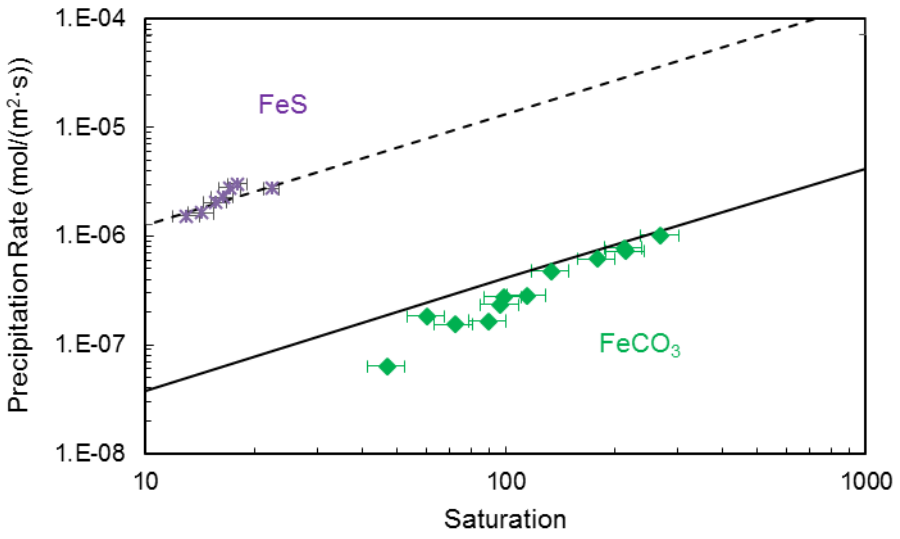

Figure 14: Precipitant rates comparison between FeS and $FeCO_3$ at 50°C.

CONCLUSIONS

- By using EQCM, repeatable and consistent $FeCO_3$ precipitation rates were obtained using different substrates, across a temperature range of 50 – 80°C. Experiments conducted on a cathodically polarized iron-coated crystal tend to minimize the influence of surface dissolution.
- FeS precipitation rate on both cathodically polarized Fe-coated quartz crystal and compensated actively corroding Fe-coated quartz crystal were in good agreement, but suffered from lack of knowledge of surface FeS saturation S_{FeS}.
- When the S_{FeS} in the bulk solution was relatively high (*ie.*, $S_{FeS,bulk} > 10$), the precipitation rate PR_{FeS} could be directly calculated by using $S_{FeS,bulk}$; at lower values, the substrate surface condition needs to be considered.
- The PR_{FeS} was found to have a weak temperature dependance as the required activation energy was 50% lower than the same for $FeCO_3$ precipitation.
- The precipitation kinetics of FeS is almost two orders of magnitude faster than that of $FeCO_3$ at the same conditions.

ACKOWLEDGEMENTS

The author would like to thank the following companies for their financial support: Anadarko, Baker Hughes, BP, Chevron, CNOOC, ConocoPhillips, DNV GL, ExxonMobil, M-I SWACO (Schlumberger), Multi-Chem (Halliburton), Occidental Oil Company, Petrobras, PTT, Saudi Aramco, Shell Global Solutions, SINOPEC (China Petroleum), TransCanada, TOTAL, and Wood Group Kenny.

REFERENCES

[1] J. Ning, Y. Zheng, D. Young, B. Brown, and S. Nešić, "Thermodynamic study of hydrogen sulfide corrosion of mild steel," *Corrosion,* vol. 70, (2014): pp. 375-389.

[2] J. Ning, Y. Zheng, B. Brown, D. Young, and S. Nešić, "Construction and verification of pourbaix diagrams for hydrogen sulfide corrosion of mild steel," CORROSION/2015, paper no. 5507, (Dallas, TX: NACE, 2015).

[3] E. W. J. v. Hunnik, B. F. M. Pots, and E. L. J. A. Hendriksen, "The formation of protective $FeCO_3$ corrosion product layers in CO_2 corrosion," CORROSION/1996, paper no. 6, (Houston, TX: NACE, 1996).

[4] W. Sun, S. Nešić, and R. C. Woollam, "The effect of temperature and ionic strength on iron carbonate ($FeCO_3$) solubility limit," *Corrosion Science,* vol. 51, (2009): pp. 1273-1276.

[5] S. Nešić and W. Sun, "Corrosion in Acid Gas Solutions," in *Shreir's Corrosion*. vol. 2, (Amsterdam: Elsevier, 2010) pp. 1270-1298.

[6] W. Sun and S. Nešić, "Kinetics of corrosion layer formation: Part 1—iron carbonate layers in carbon dioxide corrosion," *Corrosion,* vol. 64, (2008): pp. 334-346.

[7] J. Greenberg and M. Tomson, "Precipitation and dissolution kinetics and equilibria of aqueous ferrous carbonate vs temperature," *Applied Geochemistry,* vol. 7, (1992): pp. 185-190.

[8] M. L. Johnson and M. B. Tomson, "Ferrous Carbonate Precipitation Kinetics and Its Impact on CO_2 Corrosion," CORROSION/1991, paper no. 268, (Houston, TX, 1991).

[9] D. Rickard, "An apparatus for the study of fast precipitation reactions," *Mineralogical Magazine,* vol. 53, (1989): pp. 527-530.

[10] D. Rickard, "Kinetics of FeS precipitation: Part 1. Competing reaction mechanisms," *Geochimica et Cosmochimica Acta,* vol. 59, (1995): pp. 4367-4379.

[11] N. Harmandas and P. Koutsoukos, "The Formation of Iron (II) Sulfides in Aqueous Solutions," *Journal of Crystal Growth,* vol. 167, (1996): pp. 719-724.

[12] K.-L. J. Lee, "A mechanistic moceling of CO_2 corrosion of mild steel in the presence of H_2S," Ph.D. Dissertation, Dept. Chem. Eng., Ohio Univ., Athens, OH, 2004.

[13] Y. Zheng, "Electrochemical Mechanism and Model of H_2S Corrosion of Carbon Steel," Ph.D. Dissertation, Dept. Chem. Eng., Ohio Univ., Athens, OH, 2015.

[14] L. G. Benning, R. T. Wilkin, and H. L. Barnes, "Reaction Pathways in the Fe–S System Below 100°C," *Chemical Geology,* vol. 167, (2000): pp. 25-51.

[15] G. Sauerbrey, "Verwendung von Schwingquarzen zur Wägung dünner Schichten und zur Mikrowägung," *Zeitschrift für physik,* vol. 155, (1959): pp. 206-222.

[16] J. W. Mullin, *Crystallization*, 4th ed. (Oxford, U.K.: Butterworth-Heinemann, 2001.).

[17] X. Y. Liu, "Generic Mechanism of Heterogeneous Nucleation and Molecular Interfacial Effects," in *Advances in Crystal Growth Research*, (Amsterdam: Elsevier Science B.V., 2001) pp. 42-61.

[18] S. Nešić and K.-L. J. Lee, "A Mechanistic Model for Carbon Dioxide Corrosion of Mild Steel in the Presence of Protective Iron Carbonate Films—Part 3: Film Growth Model," *Corrosion,* vol. 59, (2003): pp. 616-628.

[19] Z. Ma, Y. Yang, B. Brown, S. Nešić, and M. Singer, "Investigation of precipitation kinetics of $FeCO_3$ by EQCM," *Corrosion Science*, Manuscript submitted for publication.